ACS APPLIED MATERIALS & INTERFACES

Research Article

Cite This: ACS Appl. Mater. Interfaces 2019, 11, 36497−36505

www.acsami.org

Silica-Supported Ionic Liquids for Heat-Powered Sorption Desalination

Ahmed Askalany,[†,‡] Christopher Olkis,[‡] Emilia Bramanti,[§] Dmitry Lapshin,[‡] Luigi Calabrese,[∥] Edoardo Proverbio,[∥] Angelo Freni,[§] and Giulio Santori*[,‡]

[†]Mechanical Engineering Department, Faculty of Industrial Education, Sohag University, Sohag 82524, Egypt

[‡]School of Engineering, Institute for Materials and Processes, The University of Edinburgh, Sanderson Building, The King's Buildings, Robert Stevenson Road, Edinburgh, Scotland EH9 3FB, U.K.

[§]Consiglio Nazionale delle Ricerche, Istituto di Chimica dei Composti Organometallici (CNR-ICCOM), Via G. Moruzzi, 1, Pisa 56124, Italy

[∥]Department of Engineering, University of Messina, Messina 98122, Italy

ABSTRACT: This work investigates the application of novel sorption materials to heat-powered desalination systems. Two ionic liquids 1-ethyl-3-methylimidazolium acetate (Emim-Ac) and 1-ethyl-3-methylimidazolium methanesulfonate (Emim-Oms) were impregnated in two silica supports, namely, Syloid AL-1FP and Syloid 72FP. Emim-Ac and Emim-Oms composite sorbents have been compared on morphology, water vapor sorption equilibrium, and heat of sorption. Fourier-transform infrared spectroscopy shows that the ionic liquid partly self-organizes on the silica surface. When used in a sorption desalination process powered by low grade heat at 60 °C, these composites have exceptionally high theoretical working capacities ranging from 1 to 1.7 g_{water} $g_{sorbent}^{-1}$. Experimental tests on a lab scale desalinator show that Emim-Ac/Syloid 72FP in real operating conditions can produce 25 kg_{water} $kg_{sorbent}^{-1}$ day^{-1}. To date, this yield is 2.5 times higher than the best achieved with silica gel.

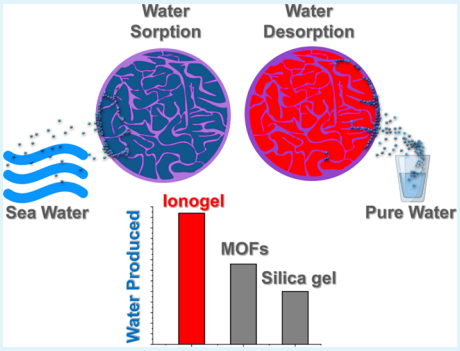

KEYWORDS: *supported ionic liquid, desalination, water, sorption, ionogel*

1. INTRODUCTION

The development of nanoporous materials for adsorption heat transformation (AHT) has increased in the last decades because of the capability of the AHT process to convert low-grade thermal energy into diverse useful effects such as cooling,[1,2] water purification,[3] atmospheric water harvesting,[4] electricity generation,[5] and long-term thermal energy storage.[6] The AHT process can be applied to water purification as schematized in Figure 1 and a more extensive description of the application can be found elsewhere.[7]

Adsorption desalination (AD) and membrane distillation (MD) are the only technological options available for desalination with low-grade heat at temperature <70 °C. A comparison on primary energy consumption between AD and MD (Figure 2) shows that MD is available in many different versions and can span a wide range of performance. MD has benefitted of large development efforts that led to commercial devices[8,9] and is currently more mature than AD. Nevertheless, the exergy efficiency of AD laboratory prototypes is competitive even with the best MD systems.

AHT devices are in practice not ready-to-market yet. The first shortfall comes from the low working capacities of the nanoporous materials used so far. The working capacity is defined as the difference in the specific amount of water sorbed [g_{water} $g_{sorbent}^{-1}$] in the sorption state (state 1 in Figure 1) and desorption state (state 3 in Figure 1) of the thermodynamic cycle. The most promising sorption materials for AHTs are called selective water sorbents (SWSs).[15] These materials are two-component systems consisting of an inorganic salt in a mesoporous silica gel matrix. Sorption equilibrium of SWSs can be tuned by changing the porous structure of the silica gels, salt type, amount of salt loaded in the host nanopores, and synthesis conditions.[16] Among the SWSs, $CaCl_2$−mesoporous silica gel[17] and LiBr−mesoporous silica gel[18] composites have unrivalled performance for heat transformation. However, such sorbents have been specifically developed for adsorption cooling purpose and do not show suitable working capacity for desalination. In fact, common commercial microporous silica gel is still the benchmarking material for desalination.[19] An early study has demonstrated that the replacement of macroporous silica gel with aerogels and xerogels results in materials such as the composite $CaCl_2$−xerogel that have exceptional equilibrium features for sorption desalination, improving the working capacity at the desalination operating conditions up to values ∼1 g_{water} $g_{sorbent}^{-1}$.[20] Unfortunately, this investigation has focused only on equilibrium measurements,

Received: May 1, 2019
Accepted: September 12, 2019
Published: September 12, 2019

DOI: 10.1021/acsami.9b07602
ACS Appl. Mater. Interfaces 2019, 11, 36497−36505

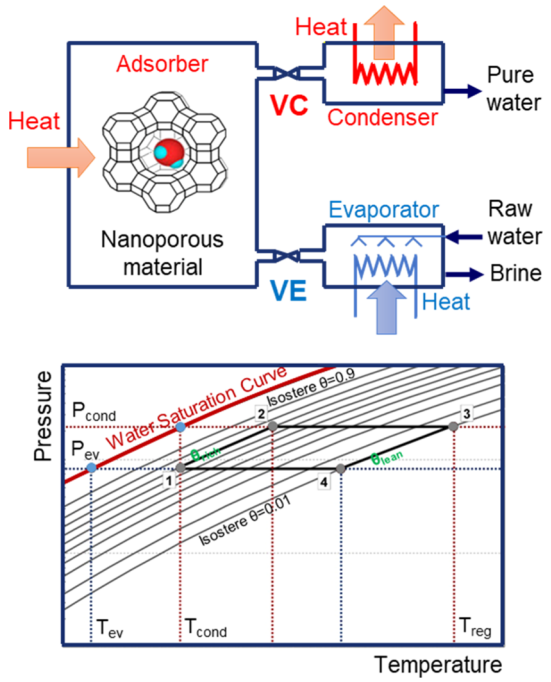

Figure 1. Scheme of a single bed AD process (top). It operates by the following two steps. Step 1 (desorption, from state 1 to state 3): Valve VC is open. The sorption material has already high water uptake (isostere θ_{rich}) and is heated in the adsorber (regeneration). After an initial heating at constant isostere (from state 1 to state 2), the water vapor released from the adsorber is condensed at ambient temperature as pure water in the condenser (from state 2 to state 3). Step 2 (adsorption, from state 3 to state 1): Valve VE connecting adsorber and evaporator are open. Valve VC connecting adsorber and condenser are closed. Heat at ambient temperature is provided to the evaporator, wherease the adsorber is kept at ambient temperature. After an initial cooling at constant isostere (from state 3 to state 4), water evaporates and is captured in the sorption material (previously regenerated by heating at isostere θ_{lean}) until state 1. Valve VE is closed. By alternating the operation of two beds (while one bed is in step 1 a second bed is in step 2), the process can be made continuous. The process follows a thermodynamic cycle (bottom) defined on three temperatures: evaporation temperature (T_{ev}), condensing temperature (T_{cond}), and regeneration temperature (T_{reg}). In AHT desalinators, evaporating, condensing, and ambient temperature are close ($T_{ev} \approx T_{cond} \approx T_{amb}$), whereas T_{reg} can be from renewable or waste heat sources and ranges from 40 to 70 °C.

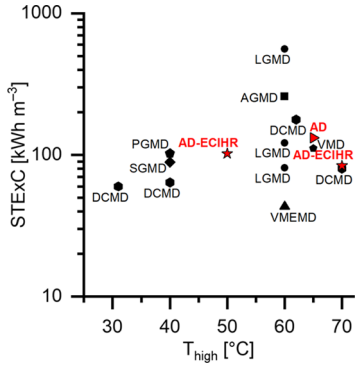

Figure 2. Comparison between AD (red symbols) and MD (black symbols) on the basis of the temperature level of the heat source (T_{high}) and the specific thermal exergy consumption (STExC). LGMD: liquid gap MD (commercial unit);[8] AGMD: air gap MD (commercial unit);[8] PGMD: permeate gap MD (laboratory unit);[10] SGMD: sweeping gas MD (laboratory unit);[10] DCMD: direct contact MD (laboratory units);[9−11] VMD: vacuum MD (laboratory unit);[12] VMEMD: vacuum multi effect MD (commercial unit);[8] AD: AD (laboratory unit using silica gel);[13] AD-ECIHR: AD evaporator/condenser heat recovery (laboratory unit using silica gel).[14]

lacking of the tests needed for the actual utilization of the material in real devices. Crystalline nanoporous materials have been also explored as materials for water-sorptive applications.[21,22] Among these, AQSOA-FAM-Z02, a chabazite type zeolite, has been initially proposed for desalination as an alternative to the benchmark amorphous silica gel.[23] Although its working capacity (~0.27 $g_{water}\ g_{sorbent}^{-1}$)[5] is attractive, it is still limited and below $CaCl_2$−xerogel. Different metal−organic frameworks (MOFs) such as MIL-101(Cr), aluminum fumarate and CPO-27(Ni) have been also investigated for desalination processes, the latter showing a working capacity of ~0.32 $g_{water}\ g_{sorbent}^{-1}$.[24] This is higher than AQSOA-FAM-Z02 but it can only be achieved when regeneration heat is available at temperatures >90 °C. High production cost and low stability upon repeated water sorption cycles are other possible issues limiting the practical use of MOFs. In addition to physisorption in nanoporous materials, many hydrophilic ionic liquids have been investigated as process fluids for thermally driven technologies.[25] In particular, 1-ethyl-3-methylimidazolium methanesulfonate (Emim-Oms) ionic liquid has shown ~0.77 $g_{water}\ g_{ionic\ liquid}^{-1}$ working capacity in desalination.[26] The drawback of ionic liquid sorbents is their need for multiple components and their corrosive character interwoven to their hydrophilicity. This limits their practical use.

In this work, we have developed a novel silica-supported ionic liquid composite material for water sorption exceeding the performance of $CaCl_2$−xerogel. Two silica support materials (Syloid AL-1FP or Syloid 72FP) are impregnated with two different hydrophilic ionic liquids (1-ethyl-3-methylimidazolium acetate, Emim-Ac or Emim-Oms). Emim-Ac composite sorbents have been compared to Emim-Oms composites. The morphology of the ionic liquids adsorbed onto silica has been investigated by scanning electron microscopy (SEM) imaging and the interactions between material components studied by infrared spectroscopy. The measurement of the equilibrium properties have allowed to assess the maximum theoretically achievable working capacity and select the best composite that has been tested in a real sorption desalination device.

2. MATERIALS AND METHODS

2.1. Sample Preparation. Emim-Oms and Emim-Ac ionic liquids with a purity ≥95.0% were purchased from Sigma-Aldrich. Syloid AL-1FP Silica and Syloid 72FP Silica were obtained from Grace. Composite materials were prepared by means of incipient wetness impregnation method.[16] Syloid silica was dried for 12 h at 120 °C before mixing with an aqueous solution of ionic liquid of 1:1 ratio on mass basis. After reaching homogeneity by magnetic stirring, water was gently evaporated from the solution at 80 °C; 60 wt % concentration of ionic liquid was attained for all the samples.

2.2. Scanning Electron Microscopy. Morphology of all batches was evaluated by a dual beam scanning electron microscope (Zeiss Crossbeam 540) by using FEG probe @2KV in high-resolution configuration, secondary electrons image by using an inlens detector.

2.3. Fourier Transform Infrared Spectroscopy. Attenuated total reflectance (ATR)−Fourier transform infrared spectroscopy (FTIR) spectra were recorded by using a PerkinElmer Spectrum One FTIR spectrophotometer, equipped with a universal ATR accessory

DOI: 10.1021/acsami.9b07602
ACS Appl. Mater. Interfaces 2019, 11, 36497−36505

Table 1. Physical Features of the Silica Supports

property	Syloid AL-1FP	Syloid 72FP
average particle size (μm)	6.5−8.1[32]	4.6−5.8[32]
bulk density (g L^{-1})	566[32]	112[32]
average pore volume (cm^3 g^{-1})	0.23−0.40[33,34]	1.2[32,34]
average pore diameter (Å)	26−30[33,34]	100−150[34−36]
Brunauer−Emmett−Teller surface area (m^2 g^{-1})	605−740[33,34]	340−405[34−36]

(diamond crystal) and TriGlycine Sulphate (TGS) detector. For each sample, 32 interferograms were recorded in order to obtain a suitable S/N ratio, averaged and Fourier-transformed to produce a spectrum with a nominal resolution of 4 cm^{-1} in the 600−4000 cm^{-1} range. The background was preliminarily recorded on the clean diamond crystal. Spectrum software (PerkinElmer) was employed to run and process the FTIR spectra.[27−29]

2.4. Thermogravimetric Analysis. Thermogravimetric (TG) analyses were carried out under nitrogen atmosphere using a Seiko EXSTAR 7200 TG/DTA instrument. TG curves were collected on samples of 5−8 mg in the temperature range from 30 to 900 °C (N_2 flow = 200 mL min^{-1}) with a heating rate of 10 °C min^{-1}.

2.5. Sorption Gravimetric Microbalance. Water sorption isotherms of silica-supported ionic liquids were measured using a gravimetric vapour sorption analyser Aquadyne DVS (Quantachrome Instruments). This device has ultrasensitive electronic microbalances with an accuracy of ±1.0 μg working in the range of 15−60 °C. Measurements at 25 °C were performed on for two pure silica supports (Syloid AL-1FP and Syloid 72FP) and four composites Emim-Oms/Syloid AL-1FP, Emim-Oms/Syloid 72FP, Emim-Ac/Syloid AL-1FP, and Emim-Ac/Syloid 72FP. Water vapor sorption of Emim-Ac/Syloid AL-1FP and Emim-Ac/Syloid 72FP was also measured in an extended temperature range between 25 and 55 °C.

2.6. Adsorption Desalinator. Emim-Ac/Syloid 72FP powder (66 g) was integrated within the aluminum heat exchanger of a lab scale AD apparatus, resulting in an ionogel monolithic structure. The adsorption desalinator has been detailed elsewhere.[30,31] The small-scale design of the test-rig enables the testing of small samples (25−200 g) of adsorption materials. The test rig was used in one-bed mode.

3. RESULTS AND DISCUSSION

3.1. Material Characterization. Table 1 reports the physical features of the two silica supports investigated in this work. Syloid FP silica are silica gels with a particularly high density of surface silanol groups (≡Si−OH), commercially used as moisture controllers in pharmaceutical and personal care products.

The two silicas were impregnated with Emim-Oms and Emim-Ac ionic liquids. These two ionic liquids were selected for their high affinity with water after the analysis of their vapor liquid equilibrium data.[37−39] Previous investigations have shown that 60 wt % impregnation of ionic liquid in the silica support is the maximal achievable impregnation and also the amount enabling the best theoretical desalination performance.[26,40] When nano-confined, ionic liquids can form ordered multilayers that functionalize the supporting surface depending on its charge.[26,41] Ordered ionic liquids have shown working capacity [g_{water} $g_{ionic\ liquid}^{-1}$] higher than disordered bulk-state ionic liquids.[26] Therefore the self-organization of the ionic liquid on the surface of a charged support is beneficial to boost the temperature-swing water sorption equilibrium properties of the ionic liquid. Usually, this special behavior shows at impregnations below 10 wt %. In this range of low impregnation, the interfacial properties of the ionic liquid are dominant over the bulk properties.[42] Impregnations below 10 wt % benefit from the interfacial properties of the ordered ionic liquids that are often advantageous for temperature swing sorption processes.[42] Nevertheless, to maximize the practical performance of a desalination device, it is beneficial to load the porous support material to completely fill the pores and the external surface of the particles. This allows higher working capacities [g_{water} $g_{sorbent}^{-1}$] than what can be achieved at low impregnation. Figure 3 shows SEM images of the pristine and impregnated Syloid 72FP silica carrier used in this study. The surface morphology of pure Syloid 72FP (sample A) is characterized by agglomerates without a regular structure with an average grain size in the range 1−5 μm (Figure 3a). At higher magnification (Figure 3b,c), the extremely fine microstructure is clearly visible. The microstructure is responsible for the large surface area in Table 1 with a highly developed network of mesopores. SEM imaging of Syloid 72FP impregnated at 60 wt % with Emim-Ac (sample B) shows that the superficial channels are still visible, although they are partially obstructed by the ionic liquid (Figure 3d−f). This is a consequence of the ionic liquid that unevenly occupies the internal porosity of the amorphous silica. The impregnation with 60 wt % Emim-Oms shows similar behavior (Figure 3g−i): the pore volume is filled with ionic liquid although the pores are only partially filled in some cases. Ionic liquid is present also on the external surface of the particles.

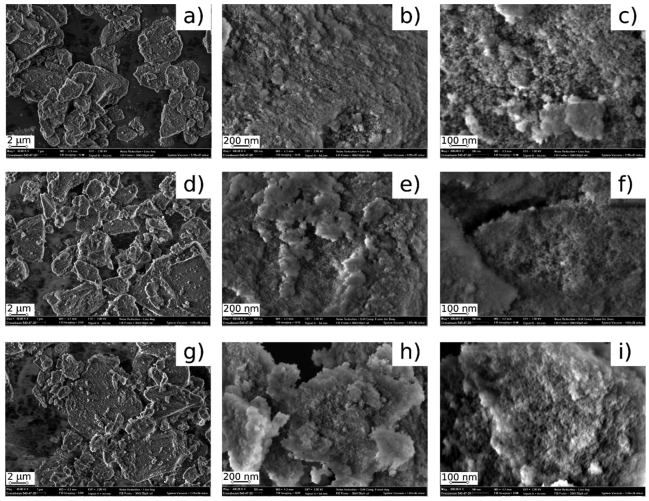

Figure 3. SEM images at different magnifications (low—40 000*x*, medium—400 000*x*, high—800 000*x*) of (a−c) sample A—Syloid 72FP, (d−f) sample B—60 wt % Emim-Ac/Syloid 72FP, (g−i) sample C—60 wt % Emim-Oms/Syloid 72FP.

ATR−FTIR spectroscopy was used to monitor the presence of Emim-Ac in Syloid 72FP and determine its interactions with the silica matrix. The ATR−FTIR spectra of pristine Emim-Ac, Syloid 72FP and 60 wt % Emim-Ac/Syloid 72FP composite are shown in Figure 4 in the 4000−600, 1750−1275, and 1275−1000 cm^{-1} range, respectively.

DOI: 10.1021/acsami.9b07602
ACS Appl. Mater. Interfaces 2019, 11, 36497−36505

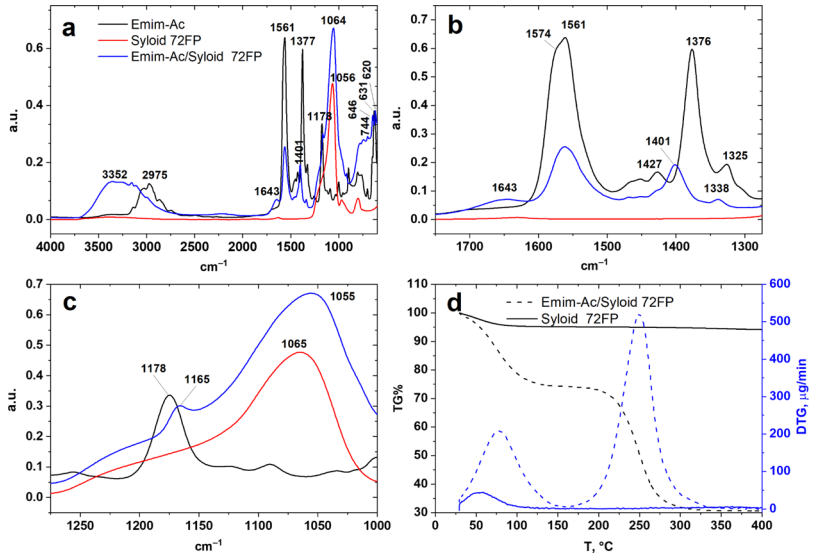

Figure 4. (a) ATR−FTIR spectra of Emim-Ac ionic liquid, Syloid 72FP, and 60 wt % Emim-Ac/Syloid 72FP composite in the (a) 4000−600, (b) 1750−1275, and (c) 1275−1000 cm^{-1} range. (d) Thermogravimetric analysis of Syloid 72FP and 60 wt % Emim-Ac/Syloid 72FP composite in the 20−400 °C temperature range.

Syloid 72FP FTIR spectrum is characterized by a broad intense Si−O absorption band at 1250−1000 cm^{-1}.[43] In the FTIR spectrum of pristine Emim-Ac (Figure 4a−c, black line), the spectral bands above 3000 cm^{-1} correspons to the C−H vibrational modes of the imidazolium ring. The bands between 2900 and 2800 cm^{-1} are because of the aliphatic asymmetric (C−H) stretching vibrations, symmetric and asymmetric stretching modes of CH_2 and CH_3, respectively. The complex band at 1561 cm^{-1} with a shoulder at 1574 cm^{-1} is because of the antisymmetric C═O stretching of acetate anion interacting with the imidazolium ring of the cation. In this specific case, no significant amounts of physisorbed water is present in pristine Emim-Ac, considering the absence of the OH stretching band around 3400 cm^{-1} and OH bending band at 1650 cm^{-1} of water. The IR vibration bands at 1376, 1178, and 1000 cm^{-1} are assigned to symmetric stretching of the C═O bond of the anion and to C−C, C−N asymmetric stretching and C−H bending vibrations of the imidazolium ring, respectively. The bands present at 1120−1000 and 940−890 cm^{-1} are because of C−O stretching and out-of-plane deformation vibrations of the acetate anion.[44] The band at 630 cm^{-1} is assigned to alkane C−H bending vibrations. The broad spectral bands at 500−600 cm^{-1} is because of the organic metal complex formation.[45]

Once loaded into the Syloid 72FP matrix, Emim-Ac strongly interacts with the silica matrix and water eventually physisorbed. As the average pore width is 10 nm and the surface of silica particles is negatively charged through silanol groups, a highly ordered structure of Emim-Ac is expected. The interaction of silica phase with Emim-Ac is confirmed by the significant shifts of the Si−O stretching band from 1065 of Syloid to 1055 cm^{-1} of Emim-Ac/Syloid 72FP likely because of the formation of hydrogen bonds between the Si−OH groups and the ionic liquid. Moreover, peaks associated with the vibrations of the acetate anion at 1376 cm^{-1} and the second derivative components at 1348, 1324, 927, 898, 1324, 927, and 898 cm^{-1} shifted toward 1401, 1360, 1338, 944, and 919^{-1} upon impregnation of the ionic liquid in the porous silica. The peaks at 1178 and 1000 cm^{-1} of the imidazolium cation shift toward 1165 and 985 cm^{-1} for the composite. These observations confirm that the imidazolium ring of the cation interacts with the negatively charged surface.

FTIR analysis shows that water adsorbs in the porous structure upon impregnation of silica with the ionic liquid (Figure 4a,b, blue line). The broad bands around 3300 and 1643 cm^{-1} observed for Emim-Ac/Syloid 72FP composite are because of the OH stretching and OH bending modes, respectively, of water molecules present in pores of the impregnated material. The abovedescribed changes in the frequency of C═O asymmetric (1561−1566 cm^{-1}) and symmetric (1376−1401 cm^{-1}) stretching modes of the acetate ion in Emim-Ac and Emim-Ac/Syloid 72FP composite are also affected by the interaction of the anion with physisorbed water. The presence of water molecules may lead to the formation of a solvation shell around the acetate anion, leading to weaker interaction between ions.

ATR−FTIR spectra of the Emim-Ac/Syloid 72FP composite after utilization in the desalination device for 500 cycles (temperature cycle 20−60 °C; 50−95% RH) did not evidence detectable alterations of the material (not shown for clarity), demonstrating its hydrothermal stability.

In the thermogravimetric analysis (TGA), the pristine Emim-Ac has shown one step thermal degradation starting at 207 °C.[46] In Figure 4d, TGA of the pristine Syloid 72FP shows ∼3% loss of sorbed water around 55 °C. The 60 wt % Emim-Ac/Syloid 72FP composite has two degradation steps at 77.1 °C (25.3% weight loss) because of water desorption and at 248.7 °C (43.4% weight loss) because of Emim-Ac, with 30.3% residual weight of the Syloid 72FP. This confirms the impregnation of Syloid with 59 ± 2 wt % Emim-Ac and the stability of the material in the operating conditions of the desalination cycle.

3.2. Water Vapor Sorption. Figure 5 shows the gravimetric measurements of water sorption equilibrium isotherms of pure Syloid AL-1FP, Syloid 72FP, and silica-supported ionic liquids impregnated at 60 wt % Emim-Oms/Syloid AL-1FP, Emim-Oms/Syloid 72FP, Emim-Ac/Syloid AL-1FP, and Emim-Ac/Syloid 72FP. The equilibrium

DOI: 10.1021/acsami.9b07602
ACS Appl. Mater. Interfaces 2019, 11, 36497−36505

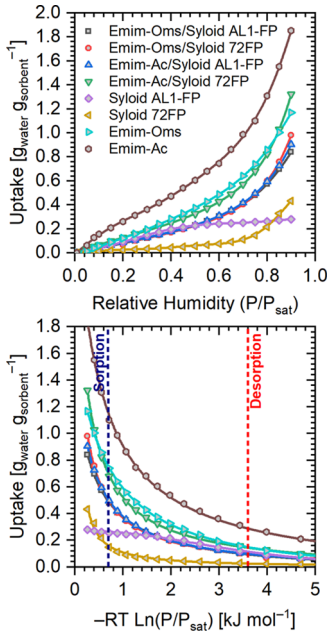

Figure 5. Experimental adsorption isotherms at 25 °C (top) from the gravimetric vapor sorption microbalance and characteristic curves (bottom) of the materials under investigation. All composite materials are impregnated with 60 wt % of ionic liquid. The dashed straight lines mark the value of $-RT\ \ln(P/P_{sat})$ at the adsorption and desorption conditions by considering a thermodynamic sorption desalination cycle with $T_{cond} = T_{sorpt} = 25$ °C; $T_{ev} = 20$ °C and $T_{reg} = 50$ °C.

isotherms are essential to the calculation of the desalination cycle in Figure 1 and accordingly to rank the material combinations on working capacity. The theoretical working capacity was calculated from the individual characteristic curves for all the preparations.[47] Emim-Ac/Syloid 72FP has the highest water vapor uptake, whereas no significant differences were observed among Emim-Oms/Syloid AL-1FP, Emim-Oms/Syloid 72FP, and Emim-Ac/Syloid AL-1FP. Table 2

Table 2. Full Factorial Analysis on Different Combinations of Ionic Liquid and Silica

silica	ionic liquid	working capacity[a] [$g_{water}\ g_{sorbent}^{-1}$]	effect[a] [$g_{water}\ g_{sorbent}^{-1}$]
Syloid AL1-FP	Emim-Oms	0.361	0.395 (mean)
Syloid 72FP	Emim-Oms	0.351	0.056 (silica)
Syloid AL1-FP	Emim-Ac	0.373	0.078 (ionic liquid)
Syloid 72FP	Emim-Ac	0.495	0.066 (interaction silica/ionic liquid)

[a]Effect of the change of each single variable (type of silica, type of ionic liquid) or binary interaction between variables (interaction silica/ionic liquid) on the working capacity.

shows a comparison of the results and their analysis through the two-level full factorial design, that is a known statistical technique.[48] In this case, the full factorial design allows to separate and quantify the effect on the working capacity of: (i) the type of support material; (ii) the type of ionic liquid and; (iii) the presence of any eventual interaction between ionic liquid and silica which would be beneficial or detrimental to the desalination performance.

Water sorption curves shown in Figure 5 demonstrate that the type of ionic liquid influences the working capacity more than other factors, increasing it by 0.078 $g_{water}\ g_{sorbent}^{-1}$ upon changing from Oms to Ac anion. This result agrees with other studies in which the Ac anion has been proved to have larger affinity with water than Oms anion.[37] Moreover, tailored silica-support properties can contribute to the increase of the working capacity. In this specific case, the working capacity increased by 0.056 $g_{water}\ g_{sorbent}^{-1}$ upon moving from Syloid AL1-FP to Syloid 72FP. By matching the results in Table 2 with the silica features in Table 1, the combination of support having large pore volume with ionic liquids having high water affinity results in composites with optimal working capacities. Figure 6 shows a more detailed analysis of the water vapor

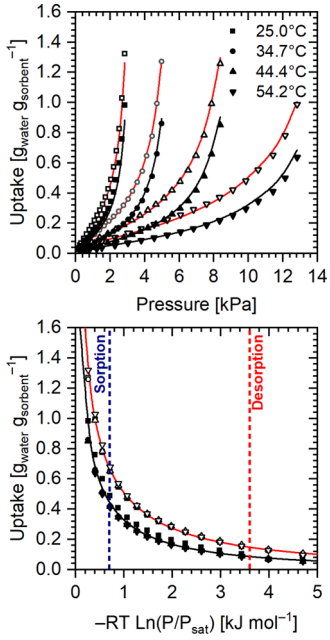

Figure 6. Experimental adsorption isotherms at 25.0, 34.7, 44.4 and 54.2 °C (top) from the gravimetric vapor sorption microbalance and characteristic curves (bottom) of Emim-Ac/Syloid 72FP (open symbols) and Emim-Oms/Syloid 72FP (filled symbols). All composite materials contain 60 wt % ionic liquid. Solid lines are from the Dubinin–Astakhov isotherm regressions. The dashed straight lines in the bottom graph mark the same sorption and desorption conditions of Figure 5.

isotherms at 25.0, 34.7, 44.4, and 54.2 °C and characteristic curves of Emim-Ac/Syloid 72FP and Emim-Oms/Syloid 72FP composites impregnated with 60 wt % ionic liquid. Solid lines are from the Dubinin–Astakhov (DA) isotherm regressions.[49]

The DA isotherm appropriately fits the experimental data and corresponds to the expression

$$w = \frac{v_0}{v_a}\exp\left\{-\left(\frac{RT}{E}\ln\left(\frac{P_{sat}}{P}\right)\right)^n\right\} \quad (1)$$

where w is the uptake [$g_{water}\ g_{sorbent}^{-1}$], v_0 the water volumetric saturation capacity [$cm_{water}^3\ g_{sorbent}^{-1}$], R the universal gas constant [kJ $kmol^{-1}$ K^{-1}], E the characteristic energy [kJ $kmol^{-1}$], P the pressure [kPa], P_{sat} the water saturation pressure [kPa] at the equilibrium temperature, and n is the isotherm regression constant. The specific volume of the

DOI: 10.1021/acsami.9b07602
ACS Appl. Mater. Interfaces 2019, 11, 36497–36505

adsorbed phase v_a [cm_{water}^3 g_{water}^{-1}] is estimated by the rectilinear diameters law[50]

$$v_a = \left(BT - \frac{1}{V_{sat}}\right)^{-1} \quad (2)$$

where v_{sat} is the water saturated vapor-specific volume [cm^3 g^{-1}] at the equilibrium temperature and B [kg m^{-3} K^{-1}] is the fitting constant. The values of the fitting parameters of the DA isotherm are reported in Table 3.

Table 3. Fitting Parameters of the DA Isotherm for the Composites Emim-Oms/Syloid 72FP Emin-Ac/Syloid 72FP Loaded with 60 wt % Ionic Liquid

parameter	unit	Emim-Oms/Syloid 72FP	Emin-Ac/Syloid 72FP
v_0	cm_{water}^3 $g_{sorbent}^{-1}$	38.78	37.06
E	J mol^{-1}	12.80	16.03
n		0.27	0.27
B	kg m^{-3} K^{-1}	0.74	0.90
AAD[a]	g_{water} $g_{sorbent}^{-1}$	0.020	0.016

[a]Average absolute deviation between experimental and calculated uptakes.

In Figure 5, the experimental data at different temperatures collapse in a single temperature-independent characteristic curve. This is an interesting feature of this type of materials because it enables the measurement of a single isotherm instead of a full set to provide enough information for quantifying the working capacity of a material in a sorption desalination cycle.

A second fundamental characteristic of optimal sorption materials is their low energy of desorption. The minimum thermodynamic desorption energy coincides with the latent heat of the specific fluid adsorbed (water in this case). Every additional interaction between water and sorbent increases the amount of binding energy, resulting in energy of desorption larger than the latent heat. The desorption energy depends on the differential sorption enthalpy curve that can be derived from the Clausius−Clapeyron equation by using the sorption isotherm, provided that the isotherm accurately fits the experimental data. For an ideal adsorbed phase, the definition of differential sorption enthalpy is

$$h_{diff} = -RT^2\left(\frac{\partial \ln P}{\partial T}\right)_{\vartheta} \quad (3)$$

The application of the definition on the DA isotherm results in

$$h_{diff} = L + E\left[\ln\left(\frac{1}{\vartheta}\right)\right]^{1/n} + \frac{ET\alpha}{n}\left[\ln\left(\frac{1}{\vartheta}\right)\right]^{1-n/n} \quad (4)$$

where $\theta = (v_a/v_0)$ is the fractional filling, L is the latent heat [kJ kg^{-1}], and α [K^{-1}] is the thermal expansion coefficient of the adsorbed fluid[50] which is

$$\alpha = v_a\left(B - \frac{\alpha_g}{v_{sat}}\right) \quad (5)$$

where α_g [K^{-1}] is the bulk vapor phase thermal expansion coefficient of water.

Figure 7 shows the trend of the net differential sorption enthalpy of Emim-Oms/Syloid 72FP and Emin-Ac/Syloid 72FP compared with a benchmarking silica gel for sorption desalination (SIOGEL).[51] The heat required to regenerate the two composites is similar and by far below that of the benchmarking silica gel. This is a further advantage of the silica-supported materials, which can provide larger working capacities at lower energy consumption. The desorption energy is almost identical to the latent heat of water over a large range of concentrations.

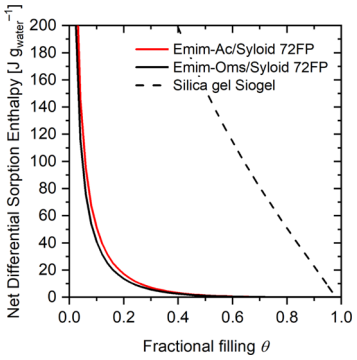

Figure 7. Comparison among the net heat of sorption (difference between differential enthalpy of adsorption and latent heat of water) of Emim-Ac/Syloid 72FP, Emim-Oms/Syloid 72FP and SIOGEL silica gel used for sorption desalination.

3.3. Application of Silica-Supported Ionic Liquids to Sorption Desalination. Sorption desalination cycles typically work at relative humidity >95%, obtained by operating at close condensation and evaporation temperatures. In all cases, water vapor sorption occurs at room temperature. In these conditions, Emim-Ac/Syloid 72FP and Emim-Oms/Syloid 72FP have high working capacity and require minimal regeneration energy. Figure 8 shows a theoretical comparison of the working capacity for a desalination cycle of ionic liquid/Syloid composites and three advanced, standard materials (SWS-1L, SIOGEL, and CPO27-Ni) assessed from the experimental isotherms.

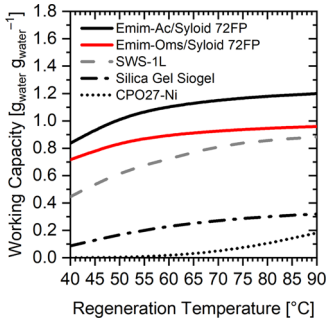

Figure 8. Comparison among the working capacity of different materials for sorption desalination vs regeneration temperatures. Cycle condition are: T_{cond} = T_{ads} = 30 °C and T_{ev} = 25 °C.

These thermodynamic calculations show that the ionic liquid/Syloid composites have good performance for desalination devices. A lab-scale sorption desalinator has been used to validate the predictions of Figure 8. Further details on the test rig can be found elsewhere.[30,31] Emim-Ac/Syloid 72FP was used at $t_{half\text{-}cycle}$ = 300 s, T_{reg} = 60 °C, inlet temperature of the heat carrier fluid to the condenser and evaporator T_{cond} = 25 °C and T_{ev} = 35 °C, respectively, where the high evaporator inlet temperature ensured that $P_{ev} \approx P_{cond}$. The half cycle time

DOI: 10.1021/acsami.9b07602
ACS Appl. Mater. Interfaces 2019, 11, 36497−36505

of 300 s was chosen on the basis of preliminary experiments, indicating that the best performance can be achieved using short cycle times. The experimental procedure is described in detail elsewhere for silica gel experiments.[31] The experimental apparatus features one evaporator, one condenser, and two adsorption beds as given in Figure 9 and operates in one-bed

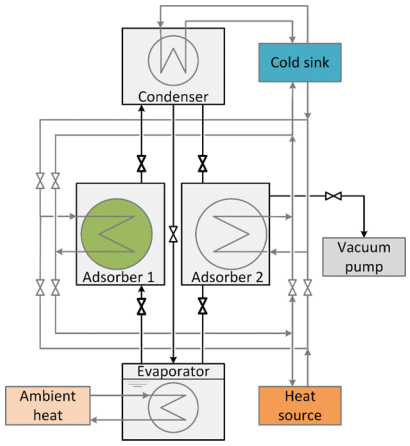

Figure 9. Schematic diagram of the adsorption test rig. The system was used in one-bed mode for the experiment presented in this study.

mode for the experiment presented here.[52] Each one of the vessels in Figure 9 contains a heat exchanger, which is connected to a thermostatic bath. Cyclic heating and cooling of the adsorption beds powers the process.

Figure 10 shows the water production based on the utilization of Emim-Ac/Syloid 72FP along with the operating relative humidity of the sorption bed. The sharp peaks in Figure 8 at the beginning of each desorption phase suggest an

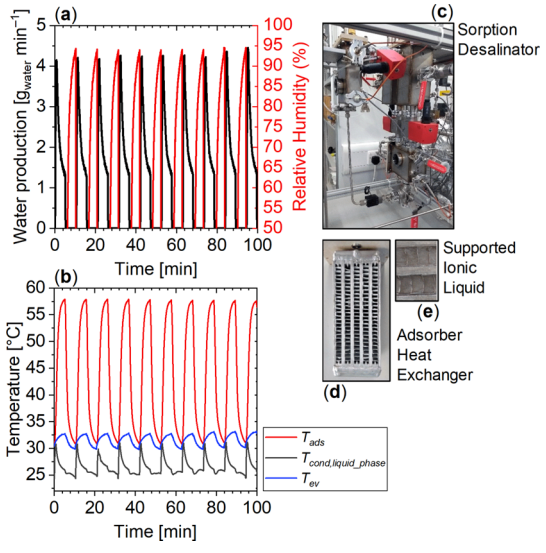

Figure 10. Experimental water production (a) with Emim-Ac/Syloid 72FP regenerated at T_{reg} = 60 °C and evolution of the temperatures (b) at the outlet of the adsorber heat exchanger (T_{ads}), of the liquid water in the condenser vessel ($T_{cond,\ liquid\ phase}$) and of the water vapor in the evaporator (T_{ev}). The value of relative humidity in (a) is calculated from the saturation pressure at T_{ads} and T_{ev}. The sorption desalinator is depicted in (c), a detail of the adsorber heat exchanger is shown in (d), whereas the supported ionic liquid integrated in the adsorber heat exchanger is shown in (e).

excellent dynamics thanks to the ionic nature of the composite sorbent. Usually sorption materials do not have good thermal conductivity and this feature makes the cycle times limited by the heat transfer. The time needed to complete a half-cycle is usually two to five times slower than those reported in Figure 10.[23,53] The experimental working capacity of the material, that is, 0.26 $g_{water}\ g_{sorbent}^{-1}$, can be further optimized to get the predicted working capacity >1.0 $g_{water}\ g_{sorbent}^{-1}$. The material can achieve higher working capacity at 95% relative humidity, which can be reached only at the end of each adsorption. Before this time, the relative humidity remains below 95% because the bed is still cooling from the previous desorption. Moreover, the evaporating water cools the evaporator down, which reduces the evaporation pressure further and makes P_{ev} unstable.

The primary performance indicator to assess the performance of an adsorption desalinator is the specific daily water production (SDWP [$kg_{water}\ kg_{sorbent}^{-1}\ day^{-1}$]), which illustrates the water throughput of a real system within 1 day over the course of many cycles

$$\mathrm{SDWP} = N\int_0^{t_{cycle}} \frac{\dot{Q}_{cond}}{L\ M_{AD}}\,dt \tag{6}$$

where N [-] is the number of cycles performed in a day, L [kJ kg^{-1}] is the latent heat of water, M_{AD} the mass of the adsorption material [kg], and Q_{cond} [kJ s^{-1}] is the condensing power

$$\dot{Q}_{cond} = \dot{m}_{cond} c_{p,w} (T_{cond,in} - T_{cond,out}) \tag{7}$$

where $\dot{m}$ is the flow rate of cooling water [kg s^{-1}] provided to the condenser heat exchanger, $c_{p,w}$ is the specific heat of the cooling water [kJ kg^{-1} K^{-1}], and $T_{cond,in/out}$ are the temperatures measured at the inlet and outlet flow of the heat exchanger [K].

Because of the fast cycles, the material was able to produce 24.9 $kg_{water}\ kg_{sorbent}^{-1}\ d^{-1}$, which is the highest experimentally validated SDWP for sorption desalination. Figure 11 shows a comparison of SDWP value for Emim-Ac/Syloid 72FP, CPO27-Ni MOF, and SIOGEL silica gel in analogous operating conditions.[5,24] SDWP of Emim-Ac/Syloid 72FP results 66% higher. Both CPO27-Ni MOF and silica gel

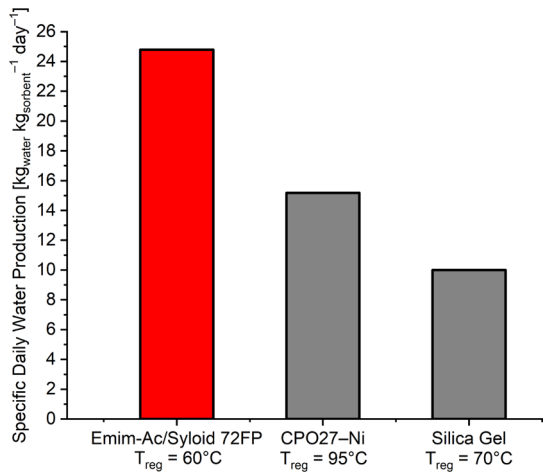

Figure 11. Comparison of the experimental SDWP of Emim-Ac/Syloid 72FP with CPO27-Ni MOF and SIOGEL silica gel. T_{reg} is the regeneration temperature applied to the sorption bed.

DOI: 10.1021/acsami.9b07602
ACS Appl. Mater. Interfaces 2019, 11, 36497−36505

require regeneration temperatures >70 °C, whereas Emim-Ac/Syloid 72P maintains good working capacity at 60 °C. This allows the utilization of ultralow grade heat sources. Thus, compared with silica gel, Emim-Ac/Syloid 72 shows a 2.5 times higher performance at lower regeneration temperature.

4. CONCLUSIONS

Four different composites with 60 wt % content of ionic liquid, namely, Emim-Oms or Emim-Ac ionic liquids supported onto Syloid AL-1FP and Syloid 72FP silica material, have been chemically characterized with SEM imaging and FTIR spectroscopy. The suitability of Emim-Ac/Syloid 72FP and Emim-Oms/Syloid 72FP for water desalination has been assessed by measuring the equilibrium in the range 25−55 °C and regressing the sorption data with a Dubinin−Astakhov model. Emim-Ac/Syloid 72FP has shown the best theoretical performance with a working capacity >1.0 $g_{water}\ g_{sorbent}^{-1}$. To validate the thermodynamic performance, the material was integrated in a lab-scale AD device.[30,31] The experimental tests have shown that in real operating conditions Emim-Ac/Syloid 72FP can produce 24.9 $kg_{water}\ kg_{sorbent}^{-1}\ d^{-1}$, which is 2.5 times higher than the benchmark silica gel at regeneration temperatures of 60 °C. To date, this material shows the highest SDWP. Therefore, supported ionic liquid composites have unrivalled properties for heat-powered desalination.

AUTHOR INFORMATION

Corresponding Author

*E-mail: g.santori@ed.ac.uk.

ORCID

Giulio Santori: 0000-0003-2156-6647

Author Contributions

The paper was written through contributions of all the authors. All the authors have given approval to the final version of the paper. Dr. G.S. is the leader and originator of the research, Dr. A.A. has prepared the materials, measured, and regressed the isotherms, Dr. C.O. has tested the material on the desalinator, Dr. A.F., Dr. E.B., and D.L. have performed FTIR and TG measurements and interpreted the results. Dr. L.C. and Prof. E.P. have performed SEM measurements.

Funding

For this research Dr. A.A., C.O., and Dr. G.S. have received funding from the EPSRC "Micro-scale energy storage for super-efficient wet appliances" project EP/P010954/1. All the remaining authors have contributed to the research supported by their home institutions.

Notes

The authors declare no competing financial interest.

ACKNOWLEDGMENTS

The research leading to these results has received funding from the EPSRC "Micro-scale energy storage for super-efficient wet appliances" project EP/P010954/1.

ABBREVIATIONS

AGMD, air gap membrane distillation
AD, adsorption desalination
AD-ECIHR, adsorption desalination with evaporator/condenser internal heat recovery
AHT, adsorption heat transformer
ATR, attenuated total reflectance
DA, Dubinin−Astakhov
DCMD, direct contact membrane distillation
Emim-Ac, 1-ethyl-3-methylimidazolium acetate
Emim-Oms, 1-ethyl-3-methylimidazolium methanesulfonate
FTIR, Fourier transform infrared spectroscopy
MD, membrane distillation
LGMD, liquid gap membrane distillation
MOFs, metal−organic frameworks
PGMD, permeate gap membrane distillation
SDWP, specific daily water production
SEM, scanning electron microscopy
SGMD, sweeping gas membrane distillation
STExC, specific thermal exergy consumption
TG, thermogravimetric analysis
VMEMD, vacuum multi effect membrane distillation
VMD, vacuum membrane distillation

REFERENCES

(1) Erdős, M.; de Lange, M. F.; Kapteijn, F.; Moultos, O. A.; Vlugt, T. J. H. In Silico Screening of Metal−Organic Frameworks for Adsorption-Driven Heat Pumps and Chillers. *ACS Appl. Mater. Interfaces* **2018**, *10*, 27074−27087.

(2) Henninger, S. K.; Habib, H. A.; Janiak, C. MOFs as Adsorbents for Low Temperature Heating and Cooling Applications. *J. Am. Chem. Soc.* **2009**, *131*, 2776−2777.

(3) Lior, N. *Advances in Water Desalination*; Wiley, 2012.

(4) Kim, H.; Rao, S. R.; Kapustin, E. A.; Zhao, L.; Yang, S.; Yaghi, O. M.; Wang, E. N. Adsorption-Based Atmospheric Water Harvesting Device for Arid Climates. *Nat. Commun.* **2018**, *9*, 1191.

(5) Olkis, C.; Santori, G.; Brandani, S. An Adsorption Reverse Electrodialysis System for the Generation of Electricity from Low-Grade Heat. *Appl. Energy* **2018**, *231*, 222−234.

(6) Li, A.; Dong, C.; Dong, W.; Atinafu, D. G.; Gao, H.; Chen, X.; Wang, G. Hierarchical 3D Reduced Graphene Porous-Carbon-Based PCMs for Superior Thermal Energy Storage Performance. *ACS Appl. Mater. Interfaces* **2018**, *10*, 32093−32101.

(7) Santori, G.; Di Santis, C. Optimal Fluids for Adsorptive Cooling and Heating. *Sustainable Mater. Technol.* **2017**, *12*, 52.

(8) Zaragoza, G.; Ruiz-Aguirre, A.; Guillén-Burrieza, E. Efficiency in the Use of Solar Thermal Energy of Small Membrane Desalination Systems for Decentralized Water Production. *Appl. Energy* **2014**, *130*, 491−499.

(9) Dow, N.; Gray, S.; Li, J.-d.; Zhang, J.; Ostarcevic, E.; Liubinas, A.; Atherton, P.; Roeszler, G.; Gibbs, A.; Duke, M. Pilot Trial of Membrane Distillation Driven by Low Grade Waste Heat: Membrane Fouling and Energy Assessment. *Desalination* **2016**, *391*, 30−42.

(10) Gao, L.; Zhang, J.; Gray, S.; Li, J.-D. Experimental Study of Hollow Fiber Permeate Gap Membrane Distillation and Its Performance Comparison with DCMD and SGMD. *Sep. Purif. Technol.* **2017**, *188*, 11−23.

(11) Bouguecha, S. T.; Aly, S. E.; Al-Beirutty, M. H.; Hamdi, M. M.; Boubakri, A. Solar Driven DCMD: Performance Evaluation and Thermal Energy Efficiency. *Chem. Eng. Res. Des.* **2015**, *100*, 331−340.

(12) Wang, Y.; Xu, Z.; Lior, N.; Zeng, H. An Experimental Study of Solar Thermal Vacuum Membrane Distillation Desalination. *Desalin. Water Treat.* **2014**, *53*, 1−11.

(13) Ng, K. C.; Thu, K.; Kim, Y.; Chakraborty, A.; Amy, G. Adsorption Desalination: An Emerging Low-Cost Thermal Desalination Method. *Desalination* **2013**, *308*, 161−179.

(14) Thu, K.; Yanagi, H.; Saha, B. B.; Ng, K. C. Performance Investigation on a 4-Bed Adsorption Desalination Cycle with Internal Heat Recovery Scheme. *Desalination* **2017**, *402*, 88−96.

(15) Freni, A.; Sapienza, A.; Glaznev, I. S.; Aristov, Y. I.; Restuccia, G. Experimental testing of a lab-scale adsorption chiller using a novel selective water sorbent "silica modified by calcium nitrate". *Int. J. Refrig.* **2012**, *35*, 518−524.

DOI: 10.1021/acsami.9b07602
ACS Appl. Mater. Interfaces 2019, 11, 36497−36505

(16) Aristov, Y. I. New Family of Solid Sorbents for Adsorptive Cooling: Material Scientist Approach. *J. Eng. Thermophys.* **2007**, *16*, 63−72.
(17) Aristov, Y. I.; Tokarev, M. M.; Cacciola, G.; Restuccia, G. Selective Water Sorbents for Multiple Applications, 1. CaCl2 Confined in Mesopores of Silica Gel: Sorption Properties. *React. Kinet. Catal. Lett.* **1996**, *59*, 325−333.
(18) Gordeeva, L. G.; Restuccia, G.; Cacciola, G.; Aristov, Y. I. Selective Water Sorbents for Multiple Applications, 5. LiBr Confined in Mesopores of Silica Gel: Sorption Properties. *React. Kinet. Catal. Lett.* **1998**, *63*, 81−88.
(19) Thu, K.; Chakraborty, A.; Saha, B. B.; Ng, K. C. Thermo-Physical Properties of Silica Gel for Adsorption Desalination Cycle. *Appl. Therm. Eng.* **2013**, *50*, 1596−1602.
(20) Mrowiec-Białoǹ, J.; Jarzębski, A. B.; Pająk, L. Water Vapor Adsorption on the SiO2-CaCl2sol-Gel Composites. *Langmuir* **1999**, *15*, 6505−6509.
(21) Ristić, A.; Logar, N. Z.; Henninger, S. K.; Kaučič, V. The Performance of Small-Pore Microporous Aluminophosphates in Low-Temperature Solar Energy Storage: The Structure-Property Relationship. *Adv. Funct. Mater.* **2012**, *22*, 1952−1957.
(22) Cadiau, A.; Lee, J. S.; Damasceno Borges, D.; Fabry, P.; Devic, T.; Wharmby, M. T.; Martineau, C.; Foucher, D.; Taulelle, F.; Jun, C.-H.; et al. Design of Hydrophilic Metal Organic Framework Water Adsorbents for Heat Reallocation. *Adv. Mater.* **2015**, *27*, 4775−4780.
(23) Youssef, P. G.; Mahmoud, S. M.; AL-Dadah, R. K. Performance Analysis of Four Bed Adsorption Water Desalination/Refrigeration System, Comparison of AQSOA-Z02 to Silica-Gel. *Desalination* **2015**, *375*, 100−107.
(24) Elsayed, E.; AL-Dadah, R.; Mahmoud, S.; Anderson, P. A.; Elsayed, A.; Youssef, P. G. CPO-27(Ni), Aluminium Fumarate and MIL-101(Cr) MOF Materials for Adsorption Water Desalination. *Desalination* **2017**, *406*, 25−36.
(25) Boman, D. B.; Hoysall, D. C.; Staedter, M. A.; Goyal, A.; Ponkala, M. J.; Garimella, S. A Method for Comparison of Absorption Heat Pump Working Pairs. *Int. J. Refrig.* **2017**, *77*, 149−175.
(26) Askalany, A. A.; Freni, A.; Santori, G. Supported Ionic Liquid Water Sorbent for High Throughput Desalination and Drying. *Desalination* **2019**, *452*, 258−264.
(27) Lenk, T. J.; Ratner, B. D.; Gendreau, R. M.; Chittur, K. K. IR Spectral Changes of Bovine Serum Albumin upon Surface Adsorption. *J. Biomed. Mater. Res.* **1989**, *23*, 549−569.
(28) Kato, K.; Matsui, T.; Tanaka, S. Quantitative Estimation of α-Helix Coil Content in Bovine Serum Albumin by Fourier Transform-Infrared Spectroscopy. *Appl. Spectrosc.* **1987**, *41*, 861−865.
(29) Bramanti, E.; Lenci, F.; Sgarbossa, A. Effects of hypericin on the structure and aggregation properties of β-amyloid peptides. *Eur. Biophys. J.* **2010**, *39*, 1493−1501.
(30) Olkis, C.; Brandani, S.; Santori, G. A Small-Scale Adsorption Desalinator. *Energy Procedia* **2019**, *158*, 1425−1430.
(31) Olkis, C.; Brandani, S.; Santori, G. Design and Experimental Study on a Small Scale Adsorption Desalinator. *Appl. Energy* **2019**, *253*, 113584.
(32) Hussain, T.; Waters, L. J.; Parkes, G. M. B.; Shahzad, Y. Microwave Processed Solid Dispersions for Enhanced Dissolution of Gemfibrozil Using Non-Ordered Mesoporous Silica. *Colloids Surf., A* **2017**, *520*, 428−435.
(33) Waters, L. J.; Hanrahan, J. P.; Tobin, J. M.; Finch, C. V.; Parkes, G. M. B.; Ahmad, S. A.; Mohammad, F.; Saleem, M. Enhancing the dissolution of phenylbutazone using Syloid based mesoporous silicas for oral equine applications. *J. Pharm. Anal.* **2018**, *8*, 181−186.
(34) Hespeler, D.; Kaltenbach, J.; Pyo, S. M. Glabridin smartPearls - Silica selection, production, amorphous stability and enhanced solubility. *Int. J. Pharm.* **2019**, *561*, 228−235.
(35) Hussain, T. *The Application of Microwave Formulation and Isothermal Titration Calorimetry for Pharmaceutical Compounds*; The University of Huddersfield, 2014.
(36) Weerapol, Y.; Limmatvapirat, S.; Jansakul, C.; Takeuchi, H.; Sriamornsak, P. Enhanced Dissolution and Oral Bioavailability of Nifedipine by Spontaneous Emulsifying Powders: Effect of Solid Carriers and Dietary State. *Eur. J. Pharm. Biopharm.* **2015**, *91*, 25−34.
(37) Römich, C.; Merkel, N. C.; Valbonesi, A.; Schaber, K.; Sauer, S.; Schubert, T. J. S. Thermodynamic Properties of Binary Mixtures of Water and Room-Temperature Ionic Liquids: Vapor Pressures, Heat Capacities, Densities, and Viscosities of Water + 1-Ethyl-3-Methylimidazolium Acetate and Water + Diethylmethylammonium Methane Sulfonate. *J. Chem. Eng. Data* **2012**, *57*, 2258−2264.
(38) Merkel, N.; Weber, C.; Faust, M.; Schaber, K. Influence of anion and cation on the vapor pressure of binary mixtures of water +ionic liquid and on the thermal stability of the ionic liquid. *Fluid Phase Equilib.* **2015**, *394*, 29−37.
(39) Krannich, M.; Heym, F.; Jess, A. Characterization of Six Hygroscopic Ionic Liquids with Regard to Their Suitability for Gas Dehydration: Density, Viscosity, Thermal and Oxidative Stability, Vapor Pressure, Diffusion Coefficient, and Activity Coefficient of Water. *J. Chem. Eng. Data* **2016**, *61*, 1162.
(40) Fehrmann, R.; Riisager, A.; Haumann, M. *Supported Ionic Liquids : Fundamentals and Applications*; Wiley-VCH, 2014.
(41) Perkin, S.; Crowhurst, L.; Niedermeyer, H.; Welton, T.; Smith, A. M.; Gosvami, N. N. Self-Assembly in the Electrical Double Layer of Ionic Liquids. *Chem. Commun.* **2011**, *47*, 6572.
(42) Henderson, Z.; Walton, A. S.; Thomas, A. G.; Syres, K. L. Water-Induced Reordering in Ultrathin Ionic Liquid Films. *J. Phys.: Condens. Matter* **2018**, *30*, 334003.
(43) Al-Oweini, R.; El-Rassy, H. Synthesis and characterization by FTIR spectroscopy of silica aerogels prepared using several Si(OR)4 and R″Si(OR′)3 precursors. *J. Mol. Struct.* **2009**, *919*, 140−145.
(44) Dhumal, N. R.; Kim, H. J.; Kiefer, J. Molecular Interactions in 1-Ethyl-3-Methylimidazolium Acetate Ion Pair: A Density Functional Study. *J. Phys. Chem. A* **2009**, *113*, 10397−10404.
(45) Jeon, Y.; Sung, J.; Seo, C.; Lim, H.; Cheong, H.; Kang, M.; Moon, B.; Ouchi, Y.; Kim, D. Structures of Ionic Liquids with Different Anions Studied by Infrared Vibration Spectroscopy. *J. Phys. Chem. B* **2008**, *112*, 4735−4740.
(46) Guyomard-Lack, A.; Buchtová, N.; Humbert, B.; Le Bideau, J. Ion Segregation in an Ionic Liquid Confined within Chitosan Based Chemical Ionogels. *Phys. Chem. Chem. Phys.* **2015**, *17*, 23947−23951.
(47) Aristov, Y. Concept of Adsorbent Optimal for Adsorptive Cooling/Heating. *Appl. Therm. Eng.* **2014**, *72*, 166−175.
(48) Di Nicola, G.; Pacetti, M.; Polonara, F.; Santori, G.; Stryjek, R. Development and Optimization of a Method for Analyzing Biodiesel Mixtures with Non-Aqueous Reversed Phase Liquid Chromatography. *J. Chromatogr. A* **2008**, *1190*, 120.
(49) Askalany, A. A.; Saha, B. B. Derivation of Isosteric Heat of Adsorption for Non-Ideal Gases. *Int. J. Heat Mass Transfer* **2015**, *89*, 186−192.
(50) Srinivasan, K.; Saha, B. B.; Ng, K. C.; Dutta, P.; Prasad, M. A Method for the Calculation of the Adsorbed Phase Volume and Pseudo-Saturation Pressure from Adsorption Isotherm Data on Activated Carbon. *Phys. Chem. Chem. Phys.* **2011**, *13*, 12559.
(51) Sapienza, A.; Velte, A.; Girnik, I.; Frazzica, A.; Füldner, G.; Schnabel, L.; Aristov, Y. ″Water - Silica Siogel″ working pair for adsorption chillers: Adsorption equilibrium and dynamics. *Renewable Energy* **2017**, *110*, 40−46.
(52) Olkis, C.; Brandani, S.; Santori, G. Cycle and Performance Analysis of a Small-Scale Adsorption Heat Transformer for Desalination and Cooling Applications. *Chem. Eng. J.* **2019**, *378*, 122104.
(53) Thu, K.; Ng, K. C.; Saha, B. B.; Chakraborty, A.; Koyama, S. Operational Strategy of Adsorption Desalination Systems. *Int. J. Heat Mass Transfer* **2009**, *52*, 1811−1816.

DOI: 10.1021/acsami.9b07602
ACS Appl. Mater. Interfaces 2019, 11, 36497−36505